Quantum local random networks and the statistical robustness of quantum scars

Federica Maria Surace, ^{1, 2} Marcello Dalmonte, ^{1, 2} and Alessandro Silva¹

¹International School for Advanced Studies (SISSA), via Bonomea 265, 34136 Trieste, Italy
²The Abdus Salam International Centre for Theoretical Physics (ICTP), strada Costiera 11, 34151 Trieste, Italy
(Dated: June 23, 2022)

We investigate the emergence of quantum scars in a general ensemble of random Hamiltonians (of which the PXP is a particular realization), that we refer to as quantum local random networks. We find two types of scars, that we call "stochastic" and "statistical". We identify specific signatures of the localized nature of these eigenstates by analyzing a combination of indicators of quantum ergodicity and properties related to the network structure of the model. Within this parallelism, we associate the emergence of statistical scars to the presence of "motifs" in the network, that reflects how these are associated to links with anomalously small connectivity (as measured, e.g., by their betweenness). Most remarkably, statistical scars appear at well-defined values of energy, predicted solely on the base of network theory. We study the scaling of the number of statistical scars with system size: below a threshold connectivity, we find that the number of statistical scars increases with system size. This allows to the define the concept of "statistical stability" of quantum scars.

Recently a great deal of research has focused on the fundamental concepts of thermalization and ergodicity shifting the focus from many-body spectra [1, 2] to the dynamics of observables [3]. A cornerstone of this program has been the formulation of the eigenstate thermalization hypothesis (ETH) [4, 5], which identifies the statistical properties of matrix elements of observables with the observation of thermal behaviour in their expectation values and correlation functions. More recently, the conditions of quantum chaos in many body systems have been further refined with the introduction of out-of-time-order correlations (OTOC) [6] and adiabatic gauge potentials [6, 7].

While two broad classes of systems have been introduced, nonergodic/localized [8, 9] vs. thermalizing [3], several systems have been shown to display intermediate behavior, where ETH is satisfied only at sufficiently high energies or for portions of the spectrum (weak ETH [10]). A prominent example in this class are quantum scars [11], that are non-ergodic eingestates embedded within the ergodic continuum. While those states are irrelevant for thermodynamics, they can still lead to very specific, intrinsically many-body phenomena in quantum quench experiments, provided the initial state has a significant overlap with them [12]. These states, which are qualitatively similar to localized states rarely occurring in the delocalized continuum of Anderson-type models [13], have been predicted in a variety of specific models [14–22], starting with constrained ones such as the PXP model [23–33].

As for localized states in the delocalized continuum, it was recently found that quantum scars of the PXP model are unstable against perturbations, suggesting that their occurrence might need fine tuning [34, 35]. It is thus presently unclear whether scarring is a robust phenomenon (and if so, in which sense), or if it generically requires parameter tuning to survive the thermodynamic limit.

While the approach to quantum scarring typically pivots around the analysis of spectral properties of 'deterministic' models, here, we pursue a different approach, and analyze the stability of scar manifolds statistically. It was already noticed that constrained models displaying scars [23] (or even shattering of the Hilbert space [36, 37]) are geometrically equivalent to networks with a number of nodes exponentially large in system size N, but an average degree per node only linear in N as a result of the locality of the Hamiltonian [24]. We build upon this analogy to define a general ensemble of Hamiltonians, called quantum local random network models, which includes the PXP model as a particular realization. Hamiltonians belonging to this ensemble are the adjacency matrices of networks whose nodes are indexed by a string of quantum numbers (e.g. {01001...}) while edges are drawn randomly with probability p only among vertices differing by local moves (spin flips): in this way, the constraints are statistically encoded in the dynamics.

We study in detail the spectra and the corresponding eigenfunctions and prove that generic Hamiltonians in this class can display two types of scars, stochastic and *statistical* which are both localized on the network. Their difference is reminiscent of the difference between size dependent [24] and exact scars [29] in the PXP model: stochastic scars occur at parameter-dependent energies which, for our models below, fluctuate wildly among different realizations, while statistical scars occur always at specific energies $\epsilon = 0, \pm 1, \pm \sqrt{2}, \pm \sqrt{3}, \pm (\sqrt{5} \pm 1)$ $1)/2, \ldots$, whose values are governed by spectral graph theory [38, 39]. A study of the scaling of the average degeneracy of statistical scars as a function of system size suggests the possible occurrence of (a series of) an eigenstate phase transition around $p_c \simeq 0.2$ between a phase in which scars proliferate and one in which their number decreases.

Quantum local random networks – The first model in which quantum scars were discovered is the PXP

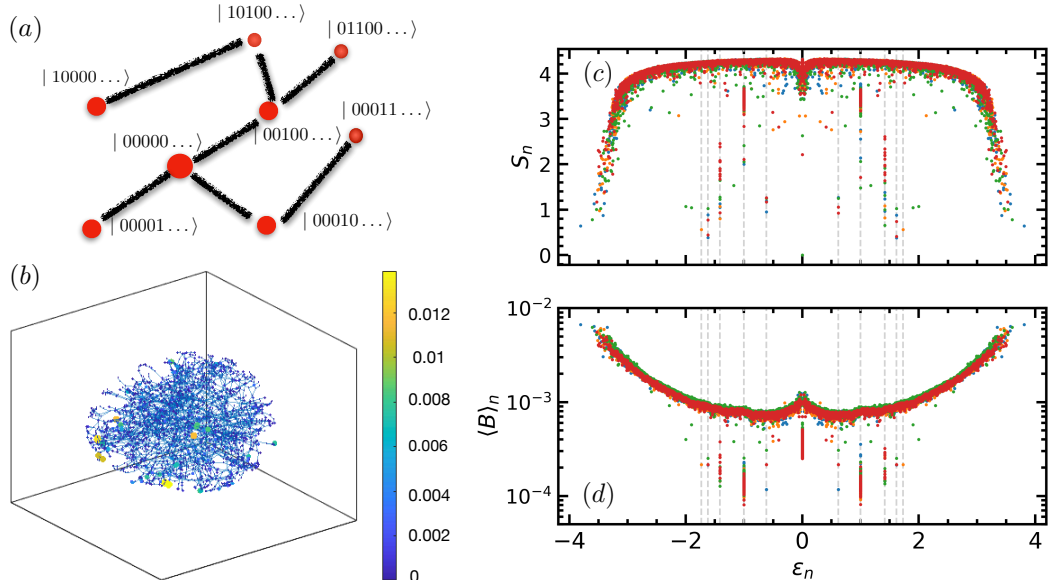


FIG. 1. (a) Illustrative example of a QLRN: states differing by a single spin flip have probability p of being connected by an edge. (b) Graphical representation of an eigenstate with $\epsilon=0$ localized in the periphery of the network for N=13, p=0.15. The color indicates the weight of the eigenstate on each node. The weight is concentrated on few nodes that are loosely connected with the rest of the network. (c) Bipartite entanglement entropy and (d) betweenness centrality of the eigenstates vs their energy for p=0.15, N=14. The different colors refer to different realizations. Dashed grey lines indicate the special energies ($\epsilon^*=\pm 1,\pm 2,\pm (\sqrt{5}\pm 1)/2,\pm \sqrt{3}$) associated with stochastic scars. At these energies, degenerate eigenstates are found, whose entanglement entropy and betweenness centrality are anomalously small with respect to the other eigenstates belonging to the thermal cloud.

model [23] which, on a chain of N sites with open boundary conditions, is defined by

$$H_{PXP} = \sum_{i=1}^{N-2} P_i X_{i+1} P_{i+2} + X_1 P_2 + P_{N-1} X_N, \quad (1)$$

where $P_i = (1-Z_i)/2$ and X_i, Z_i are local Pauli matrices. The dynamics of the PXP model is highly constrained (reflecting the microscopic mechanism of Rydberg blockade [12, 40]): it is impossible to flip a spin from down to up, if one of its nearest neighbours is up. Interestingly, the model in the subspace containing the spin-down state $|\circ\circ\circ\ldots\rangle$ can be represented as a tight-binding Hamiltonian on a specific network (Fibonacci or Lucas cube) [24].

While the majority of scars, identified through their overlap with the \mathbb{Z}_2 state $| \circ \bullet \circ \bullet \ldots \rangle$ and their low entanglement entropy, feature size-dependent effects, it was recently shown [29] that this model possesses also a few exact scar states (of the form of exact matrix product states) in the thermodynamic limit at the special energies $\epsilon = 0, \pm \sqrt{2}$. Individual scars are unstable with respect to perturbations: perturbations respecting the symmetries of the PXP model make them evaporate in the continuum of ergodic states. The instability of individual scars does not imply however that deformations of the PXP model cannot possess a scar manifold, i.e. a set of non-ergodic, low-entangled states immersed in the ergodic continuum, which are not continuous deformations of PXP scars. In this case, the existence of a scar manifold as a whole could be described as statistically stable.

In order to address such statistical stability we notice

that a common tract of constrained models is their representability as hopping Hamiltonians on networks whose nodes are indexed in the computational basis ($|\{\sigma\}\rangle$) with $\sigma = \circ, \bullet$ for the PXP model). It is therefore appealing to embed the PXP in a much broader ensemble of Hamiltonians, which we call *Quantum Local Random Networks* (QLRN) sharing the common ingredients of *locality* (in a way we specify below) and *constrained dynamics*.

Let us illustrate the construction of a QLRN in the simplest case (see Fig. [5-(a)]): consider the network whose vertices are the sequences of N elements $\{\sigma_i\}$, where $\sigma_i = 0, 1$ and $i = 1, \dots, N$, representing the computational basis of the Hilbert space of a spin system. Each pair of vertices is connected by an edge with probability $0 \le p \le 1$ provided they differ by a single flip of a boolean variable. The adjacency matrix of the resulting network is then the Hamiltonian whose spectrum and eigenfunctions will be the subject of our study. We note that, in this context, locality is intended in the sense that states connected by the Hamiltonian only differ by the properties of a single site. Evidently, while the PXP model is just a particular realization of a QLRN, we expect the latter to be mimicking the physics of the PXP model for p = 0.25 since in this model only one in four configurations of the nearest neighbours of a spin allows it to be flipped.

Note that, similarly to the PXP model, each Hamiltonian of the QLRN ensemble has matrix elements only between states with opposite Z parity, and hence anticommutes with the operator $\mathcal{C} = \prod_i Z_i$. As a conse-

quence, the spectrum is symmetric around $\epsilon=0$ and has a degeneracy in $\epsilon=0$ that scales exponentially with N [41]. Another consequence is that, from the point of view of network theory, a QLRN is locally a tree since the nearest neighbours of a vertex cannot be joined by an edge (they have the same parity), hence the clustering coefficient is always zero [42].

Localized eigenstates – The use of the language of network theory in condensed matter physics has a long history, starting from studies of Anderson-type localization in generic networks [43], disorder-free localization on random trees [38] or as a function of clustering coefficient [44, 45]. The possibility to generate localized states without disorder by taking advantage of geometrical constraints suggests that models of this type could be of interest for numerous problems, as was recently recognized in the context of the physics of many-body localization [46] and thermalization [47, 48].

For QLRN, the physics of localization emerges immediately when one considers the density of states vs. ϵ for fixed system size N at different p [49]: while for p=1 the spectrum is obviously the sequence of peaks associated to a spin of size N in unit magnetic field, as p diminishes the peaks first broaden, merging in a bell shaped DOS with a clear delta-function peak at $\epsilon=0$. This peak, also observed in the DOS of tight-binding models defined on random Erdös-Rényi networks [44], is typically associated with localized states.

In our case, the peak is a consequence of the properties of the Hamiltonian under parity symmetry, as commented above. In the case of QLRN one has to pay attention to a trivial type of localization associated to disconnected vertices which get isolated as p diminishes (a phenomenon similar to the fragmentation of Hilbert spaces observed in Ref. 36 and 50). Since in this work we will be interested in non-trivial localized states on QLRN and their connection to the physics of scars, in the following we will always identify the giant connected component of a QLRN and study localized states in this subspace. As expected a peak at $\epsilon = 0$ in its spectrum is present also under this restriction. We find that within this degenerate subspace it is possible to find non-trivial eigenstates localized on the periphery of the network as depicted in Fig. 5-(b).

The localized states at $\epsilon=0$ are just the simplest of a class of nontrivial localized states on the QLRN emerging at sufficiently small p. In order to characterize the localization properties of these and other eigenstates one may write them in the computational basis $|\Psi_n\rangle = \sum_i c_n(\{\sigma\})|\{\sigma\}\rangle$ and study the participation ratio $\mathcal{P}_n = \sum_{\{\sigma\}} |c_n(\{\sigma\})|^4$. In addition, the structure of wave functions on the QLRN can be studied using standard measures of the character of nodes: i) the degree $k(\{\sigma\})$; ii) the centrality $C(\{\sigma\}) = 1/\sum_{\sigma' \neq \sigma} l_{\sigma'\sigma}$, where $l_{\sigma'\sigma}$ is the distance between two sites on the lattice; and iii) the betweeness centrality $B(\{\sigma\})$ defined

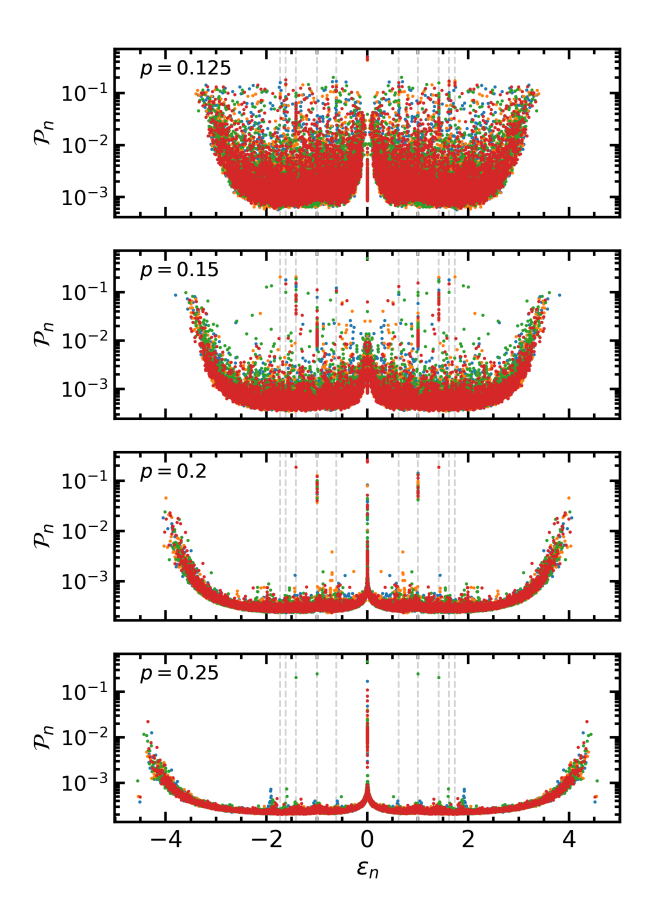


FIG. 2. Participation ratio \mathcal{P}_n of the eigenstates for different values of p for system size N=14. The colors indicate different realizations of the network. Statistical scars have large value of \mathcal{P}_n : they are localized in the computational basis. For large p their number goes to zero.

as the number of shortest paths among different vertices passing through $\{\sigma\}$. One can easily use these quantities to study eigenstates by defining their averages over a generic eigenstate $|\Psi_n\rangle$, e.g. for the betweeness

$$\langle B \rangle_n = \sum_i |c_n(\{\sigma\})|^2 b(\{\sigma\}). \tag{2}$$

Finally, since these eigenstates can be interpreted as many-body states of a spin chain of size N one may compute the half-chain entanglement entropy \mathcal{S}_n to connect localization on QLRN to the physics of scars.

As seen in Fig. 5-(c) by plotting the half-chain entanglement entropy S_n for a QLRN at p=0.15 as a function of eigenstate energy ϵ one can easily identify a number of eigenstates whose S_n is significantly lower than the typical value at that energy, therefore behaving as quantum scars. Most of these eigenstates share the feature of having significant (and untypical) participation ratio (see Fig. 6), and are therefore localized on the network. However, the way they are localized is not always the same, as shown by plotting the eigenstate average betweeness $\langle B \rangle_n$ vs. ϵ (Fig. 5-(c), lower

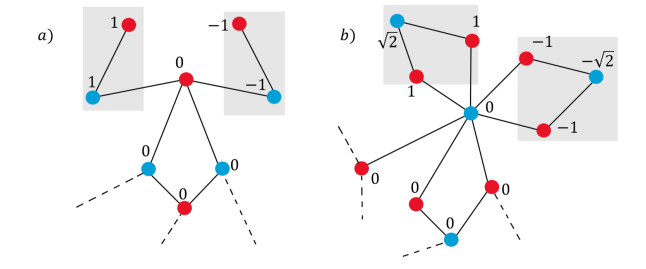


FIG. 3. Graphical representation of examples of localized eigenstates with energy (a) $\epsilon^* = 1$ and (b) $\epsilon^* = \sqrt{2}$. The color of each node indicates the parity of the corresponding state in the computational basis. Edges connect states with opposite parity. The number written on each node is the coefficient $c_n(\{\sigma\})$ of the eigenstate $|\Psi_n\rangle$ in the computational basis. Each state is localized in the grey rectangles: all other nodes have $c_n(\{\sigma\}) = 0$. In both examples, the eigenstate of the full graph is constructed using as building block an eigenstate of a small motif (of two sites in (a) and three sites in (b)): the graph contains two copies of the motif; the coefficient of the motif eigenstate are assigned with opposite signs on the two copies. The construction can be generalized to all the energies ϵ^* that are eigenvalues of small motifs.

panel): localized scars at specific energies (vertical lines at $\epsilon^* = 0, \pm 1, \pm \sqrt{2}, \pm (\sqrt{5} \pm 1)/2, \pm \sqrt{3}, \ldots$) tend to have a lower betweeness than the rest, indicating that they are not just localized, but localized on the periphery of the network. Those are the key featurs that define statistical scars: oppositely, stochastic scars occur at system size and realization dependent energies, and are not necessarily localized at the edges of the network or have low betweenness. As shown in Fig. 6, both types of scars proliferate as p is lowered below a certain threshold $p \simeq 0.2$.

Statistical scars – We now further investigate the presence of statistical scars at specific energies. The special energies ϵ^* are well known to be the eigenvalues of the adjacency matrices of small trees [38, 39]. The fact that various figures of merit, including the centrality and degree [49], suggest that statistical scars are localized on the periphery of the network, indicates that small elementary subgraphs (motifs) might be the basic elements associated to statistical scars. This is indeed the case as shown in Fig. 3: the eigenfunction of subgraphs of two vertices (eigenvalues ± 1) or three vertices (eigenvalues $\pm \sqrt{2}$,0) can be easily incorporated into eigenfunctions of the whole QLRN whenever geometrical structures of the type of Fig. 3-a or Fig. 3-b occur on its periphery.

The occurrence of network motifs associated to statistical scars depends both on the overall system size N and, most crucially, on p. In order to investigate how many scars are to be expected as a function of system size, we studied how the degeneracy of statistical scars with a given value of ϵ^* , averaged over realizations of the QLRN, scales with N for a fixed p. This is shown in Fig. 4 for $\epsilon^* = 1$: while for p = 0.25 the degeneracy of

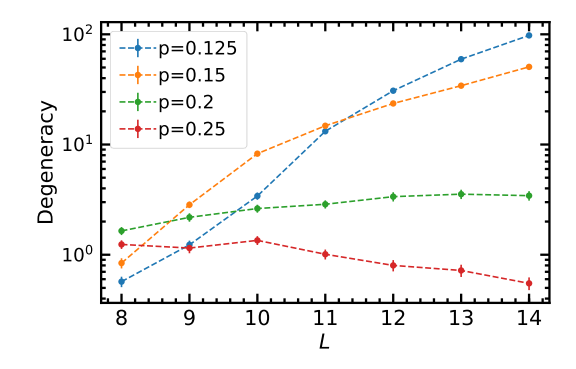


FIG. 4. Average degeneracy of the eigenspace with $\epsilon^* = 1$ as a function of system size N. For $p < p_c$ ($p_c \simeq 0.2$) the degeneracy increases with N, while it decays for $p > p_c$.

these scars does not increase with N, a completely different behavior, characterized by a continuous growth, is seen for smaller p. This fact seems to suggest the presence of an eigenstate transition as a function of p, with a critical $p_c(\epsilon=1)\simeq 0.2$. A similar behaviour is observed for other values of ϵ^* [49]. We note that, differently from eigenstate phase transitions in the context of many-body localization, in the present case, the transition occurs at exactly known values of the energy only, and not in a continuous part of the spectrum. This may facilitate future studies, targeting, e.g., exact energy manifolds.

As a last comment, we note that some of the characteristic energies of statistical scars correspond to the energies of the exact scars found in the PXP [29] and in the generalized PXP models [35]. This is not a coincidence: those scars, of the form of matrix product states (MPS), realize an effective "decoupling" of the system in small blocks; the eigenenergies are then originated from the diagonalization of the small blocks, akin to the motifs of statistical scars. Despite this similarity, we do not find a direct connection between the two types of scars. In contrast with statistical scars, the number of MPS scars does not grow with the size of the system; moreover, the structure of MPS scars is specific of the low dimensionality of the model. We leave the question of a deeper connection between the two types of scars to future works.

Conclusions and outlook – We studied the statistical stability of a scar manifold by introducing a class of Hamiltonians, Quantum Local Random Networks, that combine locality and constrained dynamics, and whose PXP is a particular instance. Focusing on the giant connected component of a QLRN we have shown that it is expected to display two types of scars for sufficiently small p: stochastic scars, which occur at realization and system size dependent energies, and statistical scars which occur at special energies, $\epsilon^* = 0, \pm 1, \pm \sqrt{2}, \pm (\sqrt{5} \pm 1)/2, \pm \sqrt{3}, \ldots$ The latter are solely dictated by random graph theory, and are associated to localized states on

certain geometrical motifs on the periphery of the QLRN. A study of the degeneracy of statistical scars for various p as a function of systems size indicates the possibility of a quantum phase transition occurring at a critical value $p_c \simeq 0.2$ between a phase in which scars proliferate and one in which their number saturates for increasing N. These states appear in a variety of specific realizations, from (generalized) PXP [29, 35] to Hubbard models [51]. Studying in detail this phenomenon, together with potential generalizations to other QLRN, is an intriguing perspective, that we leave to future investigations.

We thank G. Giudici and J. Goold for discussions, E. Gonzales Lazo and M. Votto for collaboration on related work, and A. Lerose for comments on the manuscript, and for pointing Ref. [51] to us. The work of FS and MD is partly supported by the ERC under grant number 758329 (AGEnTh), by the MIUR Programme FARE (MEPH), and by the European Union's Horizon 2020 research and innovation programme under grant agreement No 817482 (Pasquans).

- O. Bohigas, M. J. Giannoni, and C. Schmit, Phys. Rev. Lett. 52, 1 (1984).
- [2] D. Poilblanc, T. Ziman, J. Bellissard, F. Mila, and G. Montambaux, Europhysics Letters (EPL) 22, 537 (1993).
- [3] L. D'Alessio, Y. Kafri, A. Polkovnikov, and M. Rigol, Advances in Physics 65, 239 (2016), https://doi.org/10.1080/00018732.2016.1198134.
- [4] J. M. Deutsch, Phy. Rev. A 43, 2046 (1991).
- [5] M. Srednicki, Phys. Rev. E 50, 888 (1994).
- [6] A.Kitaev, "A simple model of holography," http://online.kitp.ucsb.edu/online/entangled15/ kitaev2/. (2015).
- [7] M. Pandey, P. W. Claeys, D. K. Campbell, A. Polkovnikov, and D. Sels, Phys. Rev. X 10, 041017 (2020).
- [8] F. H. L. Essler and M. Fagotti, Journal of Statistical Mechanics: Theory and Experiment 2016, 064002 (2016).
- [9] D. A. Abanin, E. Altman, I. Bloch, and M. Serbyn, Rev. Mod. Phys. 91, 021001 (2019).
- [10] G. Biroli, C. Kollath, and A. M. Läuchli, Phys. Rev. Lett. 105, 250401 (2010).
- [11] M. Serbyn, D. A. Abanin, and Z. Papić, Nature Physics 17, 675 (2021).
- [12] H. Bernien, S. Schwartz, A. Keesling, H. Levine, A. Omran, H. Pichler, S. Choi, A. S. Zibrov, M. Endres, M. Greiner, V. Vuletic, and M. D. Lukin, Nature 551, 579 (2017).
- [13] S. Kirkpatrick and T. P. Eggarter, Phys. Rev. B 6, 3598 (1972).
- [14] S. Moudgalya, S. Rachel, B. A. Bernevig, and N. Regnault, Phys. Rev. B 98, 235155 (2018).
- [15] M. Schecter and T. Iadecola, Phys. Rev. Lett. 123, 147201 (2019).
- [16] S. Moudgalya, E. O'Brien, B. A. Bernevig, P. Fendley, and N. Regnault, Phys. Rev. B 102, 085120 (2020).

- [17] O. Hart, G. De Tomasi, and C. Castelnovo, Phys. Rev. Research 2, 043267 (2020).
- [18] D. K. Mark, C.-J. Lin, and O. I. Motrunich, Phys. Rev. B 101, 195131 (2020).
- [19] K. Bull, I. Martin, and Z. Papić, Phys. Rev. Lett. 123, 030601 (2019).
- [20] K. Lee, R. Melendrez, A. Pal, and H. J. Changlani, Phys. Rev. B 101, 241111 (2020).
- [21] T. Iadecola and M. Schecter, Phys. Rev. B 101 (2020), 10.1103/PhysRevB.101.024306.
- [22] N. Shiraishi and T. Mori, Physical Review Letters 119 (2017), 10.1103/PhysRevLett.119.030601, arXiv:1712.01999.
- [23] I. Lesanovsky and H. Katsura, Phys. Rev. A 86, 041601 (2012).
- [24] C. J. Turner, A. A. Michailidis, D. A. Abanin, M. Serbyn, and Z. Papić, Nat. Phys. 14, 745 (2018).
- [25] C. J. Turner, A. A. Michailidis, D. A. Abanin, M. Serbyn, and Z. Papić, Phys. Rev. B 94, 155134 (2018).
- [26] V. Khemani, C. R. Laumann, and A. Chandran, Phys. Rev. B 99, 161101 (2019).
- [27] S. Choi, C. J. Turner, H. Pichler, W. W. Ho, A. A. Michailidis, Z. Papić, M. Serbyn, M. D. Lukin, and D. A. Abanin, Phys. Rev. Lett. 122, 220603 (2019).
- [28] W. W. Ho, S. Choi, H. Pichler, and M. D. Lukin, Phys. Rev. Lett. 122, 040603 (2019).
- [29] C.-J. Lin and O. I. Motrunich, Phys. Rev. Lett. 122, 173401 (2019).
- [30] T. Iadecola, M. Schecter, and S. Xu, Physical Review B 100, 184312 (2019).
- [31] A. A. Michailidis, C. J. Turner, Z. Papić, D. A. Abanin, and M. Serbyn, Phys. Rev. X 10, 011055 (2020).
- [32] C.-J. Lin, V. Calvera, and T. H. Hsieh, Phys. Rev. B 101, 220304 (2020).
- [33] F. M. Surace, P. P. Mazza, G. Giudici, A. Lerose, A. Gambassi, and M. Dalmonte, Phys. Rev. X 10, 021041 (2020).
- [34] C.-J. Lin, A. Chandran, and O. I. Motrunich, Phys. Rev. Research 2, 033044 (2020).
- [35] F. M. Surace, M. Votto, E. G. Lazo, A. Silva, M. Dalmonte, and G. Giudici, Phys. Rev. B 103, 104302 (2021).
- [36] P. Sala, T. Rakovszky, R. Verresen, M. Knap, and F. Pollmann, Phys. Rev. X 10, 011047 (2020).
- [37] S. Moudgalya, A. Prem, R. Nandkishore, N. Regnault, and B. A. Bernevig, "Thermalization and its absence within krylov subspaces of a constrained hamiltonian," (2019), arXiv:1910.14048 [cond-mat.str-el].
- [38] O.Golinelli, "Statistics of delta peaks in the spectral density of large random trees," (2003), arXiv:0301437 [cond-mat].
- [39] S. H. Cvetkovic D.M, Doob M., Spectra of Graphs: Theory and Applications (Academic Press, New York, 1980).
- [40] D. Jaksch, J. I. Cirac, P. Zoller, S. L. Rolston, R. Cote, and M. D. Lukin, 10.1103/PhysRevLett.85.2208, quantph/0004038.
- [41] M. Schecter and T. Iadecola, Physical Review B 98, 35139 (2018), arXiv:1801.03101.
- [42] A. Barrat, M. Barthélemy, and A. Vespignani, *Dynami-cal Processes on Complex Networks* (Cambridge University Press, 2008).
- [43] M. Sade, T. Kalisky, S. Havlin, and R. Berkovits, Phys. Rev. E 72, 066123 (2005).
- [44] M. Bauer and O. Golinelli, Phys. Rev. Lett. 86, 2621 (2001).

- [45] L. Jahnke, J. W. Kantelhardt, R. Berkovits, and S. Havlin, Phys. Rev. Lett. 101, 175702 (2008).
- [46] F. Pietracaprina and N. Laflorencie, Annals of Physics , $168502\ (2021).$
- [47] D. Nickelsen and M. Kastner, Phys. Rev. Lett. 122, 180602 (2019).
- [48] D. Nickelsen and M. Kastner, Quantum 4, 273 (2020).
- [49] see supplemental material.
- [50] V. Khemani, M. Hermele, and R. Nandkishore, Phys. Rev. B 101, 174204 (2020).
- [51] J.-Y. Desaules, A. Hudomal, C. J. Turner, and Z. Papić, Phys. Rev. Lett. 126, 210601 (2021), 2102.01675.

Supplemental material

In this Supplemental Material, we provide additional information on the definition and spectra of QLRN discussed in the main text.

Generalized Quantum Local Random Networks

The notion of QLRN can be generalized to encompass situations in which either the elementary degrees of freedom are not spin 1/2 or the number of spins flipped locally is larger than one, as in Ref. 36 and 50, maintaining locality and constrained dynamics.

For concreteness, let us consider the set of sequences $\{\sigma_i\}$, where $i=1,\ldots,N$ and $\sigma_i=\{0,\ldots,q\}$, $\{q \text{ is a }$ positive integer). Two nodes $\{\sigma_i\}$ and $\{\sigma'_i\}$ are connected with probability $0 \le p \le 1$ if: i) - the string $\{\sigma_i - \sigma_i'\}$ has nonzero entries only locally, i.e. in a compact interval of finite size $L_0 \leq N$ and ii) - the distance $\sum_i |\sigma_i - \sigma'_i| \leq S_0$. The random local Hamiltonian associated to this network is then its adjacency matrix and the resulting ensemble of Hamiltonians will be denoted as $\mathcal{H}_p(L_0, S_0)$. Note that if $S_0 \geq 2$ in general the Hamiltonian does not anticommute with the total parity. It is evident that if q = 1, $L_0 = 1$ and $S_0 = 1$ we have the special case discussed in the main text and that the PXP Hamiltonian is just one of the realizations in $\mathcal{H}_p(1,1)$. Networks with larger local Hilbert space $q, S_0 > 1$ and more complex spin flips $L_0 >$ 1 are naturally related for example to spin-1 models [36] or fermionic models [50], whose analysis is left for future work.

Spectra of QLRN

Let us now consider the spectra of QLRN as a function of p as shown in Fig. (5) for N=12. When p=1 all states that can be connected by a single spin flip are connected and the Hamiltonian is $H=\sum_i \sigma_i^x$: the resulting spectrum is therefore trivial, highly degenerate with eigenvalues $\epsilon_i=N-2i$, with $i=0,\ldots,N$, and degeneracy $D_i=\binom{N}{i}$ (see Fig. (5-a)). Introducing a slight

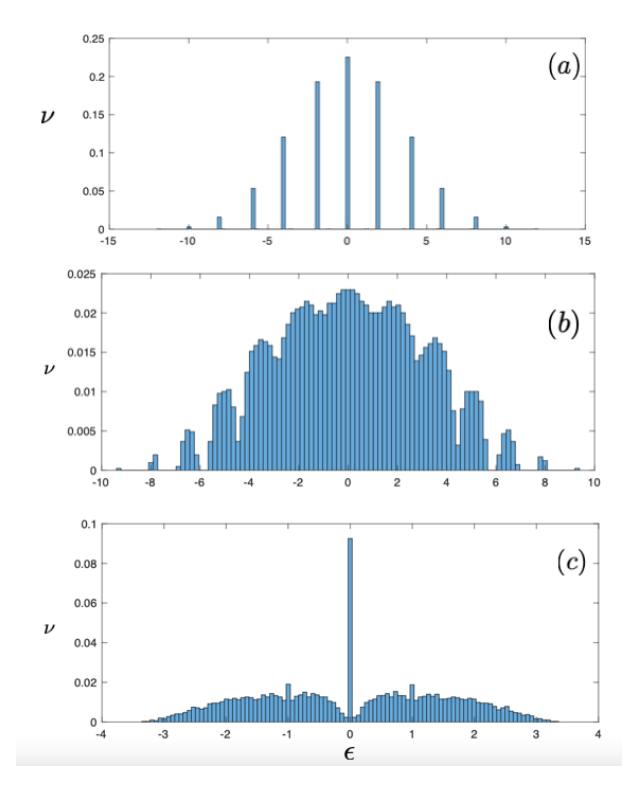


FIG. 5. Histograms of the density of states ν vs. energy ϵ of the eigenstates for a QLRN with N=12 and p=1 (panel a), p=0.75 (panel b), and p=0.15 (panel c).

stochasticity in the selection of edges splits the degeneracies leading to a characteristic spectrum similar to that shown in Fig. (5-b) for p=0.75. A further reduction of p leads to a fragmentation of the Hilbert space: in the network representation one observes a giant connected component and a few disconnected nodes associated to a peak at $\epsilon=0$ as well as, for sufficiently small p (Fig. (5-c) for p=0.15), pairs of nodes connected by an edge (peaks at ± 1 in Fig. (5-c) in the histogram of the eigenvalues)

Localization is expected to occur when p is sufficiently small. Of course there is a trivial localization related to wave functions completely localized in small disconnected components which will contribute to the peaks at $\epsilon = 0$ and $\epsilon = \pm 1$ in Fig. (5-c). A much more interesting type of localization is however happening in the giant connected component of the network that contains most of the nodes: as shown in Fig. (6) the peak at $\epsilon = 0$ persists also in this case. A visualization of the weights of the corresponding wave functions in the network, shows that these localized states are associated to wave functions with large amplitudes on nodes at the boundaries of the network. Qualitatively similar results are obtained for different N.

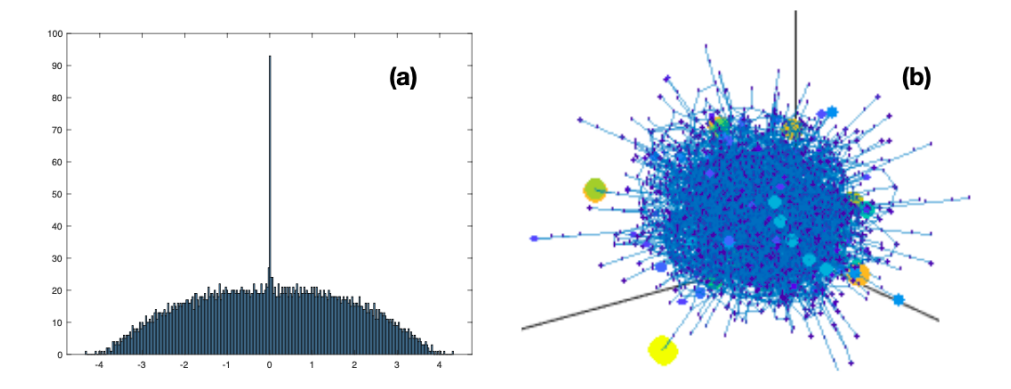


FIG. 6. (a) Histogram representation of the spectrum of the giant connected component for a QLRN with N=12 and p=0.25. The peak at $\epsilon=0$ is still visible and is associated to wavefunctions mainly localized on the periphery of the network as shown in panel (b).

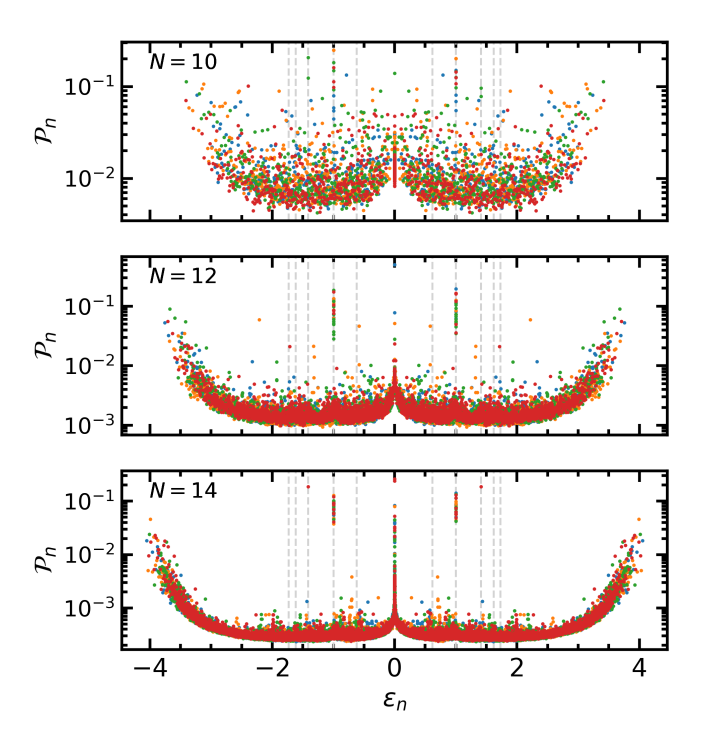


FIG. 7. Participation ratio \mathcal{P}_n of the eigenstates for p=0.2 and different system sizes N.

Participation ratio and system size

In Fig. (7) we plot the participation ratio of the eigenstates for different values of the system size N. We note that, as N is increased, the majority of the eigenstates get closer to a smooth dependence of \mathcal{P} on the energy ϵ (the thermal cloud). Statistical scars, instead, remain well isolated, with strongly non-thermal values.

Centrality and degree of statistical scars

The characterization of the localization of stochastic and statistical scars done in the main text with the participation ratio \mathcal{P}_n and the betweeness B_n can be done using other figures of merit such as the degree and the centrality of the eigenstates, defined as

$$\langle k \rangle_n = \sum_i |c_n(\{\sigma\})|^2 k(\{\sigma\}), \qquad (3)$$

$$\langle C \rangle_n = \sum_{i}^{i} |c_n(\{\sigma\})|^2 C(\{\sigma\}). \tag{4}$$

As shown in Fig. (8), statistical scars are characterized by anomalously small values of both quantities.

Eigenstate phase transition at different ϵ^*

In the main text, we discussed for the presence of an eigenstate phase transition based on the degeneracy of statistical scars at $\epsilon^* = 1$. It is possible to extend this picture to all network-predicted values of quantized energies.

In Fig. 9, we show the degeneracy scaling versus system size for four additional values of ϵ^* . For p < 0.2, we consistently observe that degeneracy is increasing with system size (due to the absence of a decade of sizes, we refrain from commenting on the precise scaling function). For p = 0.2, we observe few degeneracies, and the data seem consistent with a decreasing degeneracy for all ϵ^* . For p = 0.25, we observe a similar behavior, modulo the fact that for several data sets, we do not observe any degeneracy at all.

The overall picture seems to suggest that an eigenstate transition occurs for all values of ϵ^* , and that

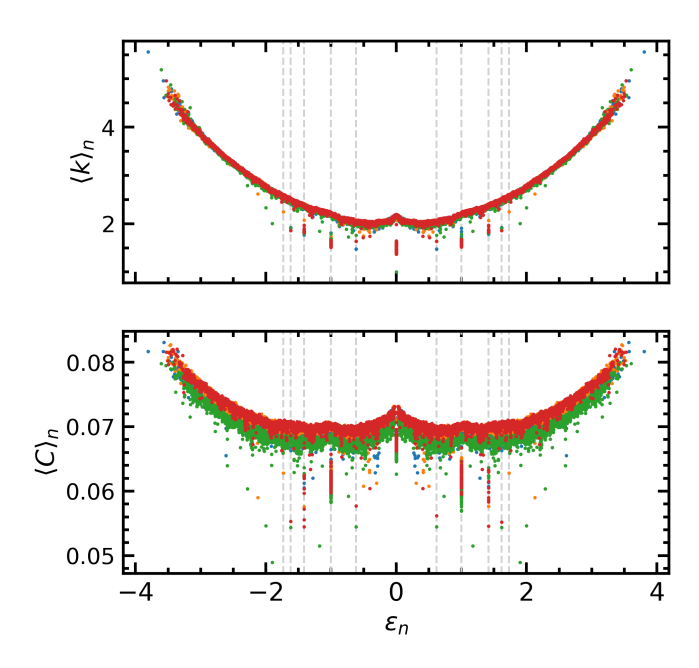


FIG. 8. Degree $\langle k \rangle_n$ and centrality $\langle C \rangle_n$ of the eigenstates as a function of their energy ϵ_n . Different colors refer to different realizations of the network. Statistical scars are chacterized by small values of both $\langle k \rangle_n$ and $\langle C \rangle_n$.

the transition point, for all cases, is located between 0.15 . Larger system sizes and more comprehensive numerics will be needed to determine whether all transitions happen at the same critical value of <math>p, or if they are energy-dependent.

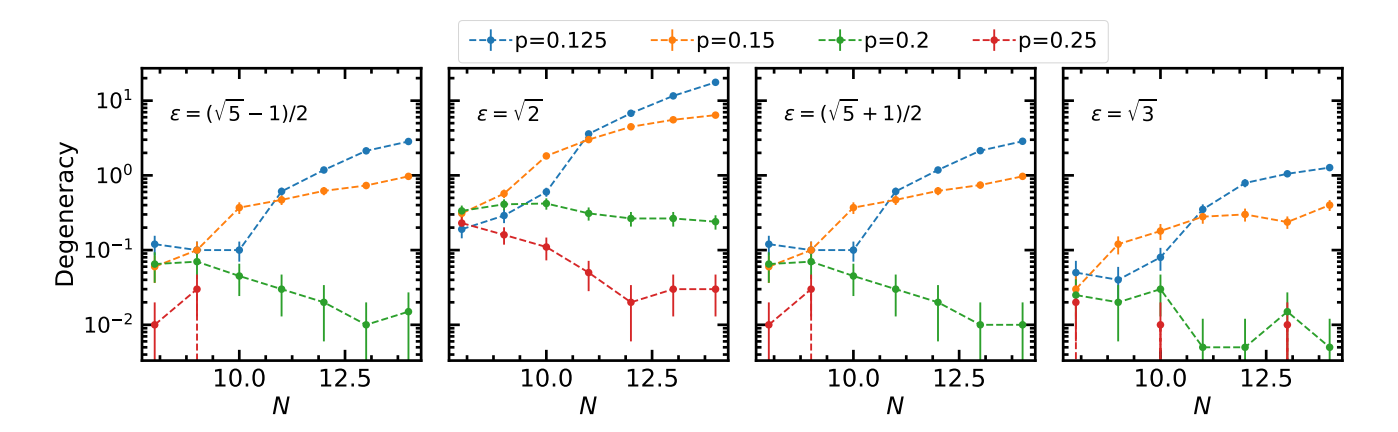


FIG. 9. Degeneracy of statistical scars vs. system size N for different p for 100 realizations of the QLRN. Statistical scars show qualitatively, though less clearly, the same behaviour as those with $\epsilon^{\star}=1$: up to $p\simeq 0.2$ their number appears to grow with system size while for larger p one observes saturation.